Pergamon

Int. J. Multiphase Flow Vol. 23, No. 6, pp. 1043–1062, 1997

Printed in Great Britain
PII: S0301-9322(97)00024-4
0301-9322/97 $17.00 + 0.00

KINEMATIC MIXING OF TWO FLUIDS WITH VALVE PERTURBATION

M. D. MAT and O. J. ILEGBUSI
Department of Mechanical, Industrial and Manufacturing Engineering, Northeastern University, Boston, MA 0215, U.S.A.

(Received 10 October 1996; in revised form 30 March 1997)

Abstract—A numerical study is presented of the effects of valve on mixing characteristics of two fluids inside a closed two-dimensional cavity. A two-fluid model is employed which involves solution of separate transport equations for zone-averaged variables of each fluid with allowance for interface friction. The calculations are performed over the parameter range: Grashof number (1–3.6×10^5), Atwood number (5×10^{-5}–0.33) and valve speed (0.025–0.1 m/s). The mixing efficiency is presented as a function of valve speed and the dynamical system characteristics of the flow field are discussed in terms of the time histories, phase space trajectories and power spectra of the velocities at a fixed point. The effects of valve and buoyancy forces are found to be comparable at high Grashof numbers and moderate valve speeds. However, the perturbation induced by the valve dominates the mixing at low Grashof numbers. © 1997 Elsevier Science Ltd.

Key Words: kinematic mixing, buoyancy, valve perturbation, two-fluids model, mixing efficiency, chaotic mixing

1. INTRODUCTION

Fluid mixing by buoyancy forces has received considerable attention because of its relevance in many applications including materials processing, atmospheric transport and oceanography. A typical example of such flow situation is the Rayleigh–Taylor instability (RTI). We present a numerical study of a model RTI problem consisting of two fluids initially separated by a vertical plate (valve) in a two-dimensional enclosure. Such arrangement is particularly relevant to the solution crystal growth method in materials processing, and for laboratory study of the interface regions of the mushy zone in alloy solification, the entrainment process at the plasma/ambient gas interface in a plasma reactor, and mixing of reactants in combustors. After removal of the valve vertically upwards, mixing occurs between the fluids at the left and right sections of the cavity due to the combined effects of the potential energy of the system and the perturbation or kinetic energy induced by the valve. This paper deals primarily with the effect of valve removal on the mixing characteristics.

The early numerical and experimental studies on Rayleigh–Taylor instability were concerned mainly with the growth of initial perturbation at the interface, overturning mechanism and effects of fluid properties such as surface tension on interface growth (Taylor 1950; Lewis 1950; Emmons *et al.* 1960; Duff *et al.* 1962). Some of the experimental studies involved placing two fluids initially in a stably-stratified condition without a valve and accelerating them downward to initiate mixing (Lewis 1950; Read 1984; Youngs 1989). Duff *et al.* (1962) studied two fluids separated by a valve in unstable conditions and showed that a threshold speed was required for the perturbation introduced by valve removal to be significant. This effect was however neglected from their theoretical work.

Linden and Redondo (1991) extended the mixing width approach first introduced by Youngs (1984) and later employed by Andrews and Spalding (1990) by experimentally studying two fluids separated by a removable aluminum valve in a three-dimensional cavity. It was found that the perturbation due to valve removal was effective only at small Atwood numbers, but the width of the mixing region grew faster in the vicinity of the surface through which the valve was removed,

irrespective of Atwood number. In the numerical study of Linden *et al.* (1994), the valve effect was approximated as an additional sinusoidal perturbation but the finite removal time and circulation induced by the valve were neglected. Thus the study showed that while initial flow development and interface evolution were affected by the valve, the degree of mixing remained unchanged.

Buoyancy-driven mixing of two fluids in a closed two-dimensional cavity in the absence of valve has been studied numerically by Duval (1992). By assuming Boussinesq fluid and low Atwood number, three basic mixing regimes were identified depending on the parametric range of Grashof number. These regimes were classified as chaotic (at large Grashof numbers), convective (at intermediate Grashof numbers) and diffusive (at low Grashof numbers). Ilegbusi *et al.* (1997) have recently predicted similar flow patterns with a non-Boussinesq two-fluid model, based on the numerical approach of Andrews (1995). In another study (Ilegbusi *et al.* 1996) found that Atwood number significantly affects the interface behavior and flow pattern at relatively large Grashof numbers. Specifically, a tendril structure develops at low Atwood numbers while a whorl structure occurs at large Atwood numbers. However, both studies (Ilegbusi *et al.* 1996, 1997) considered instantaneous valve removal and the effect of the valve on the mixing was neglected.

The objective of this paper is to extend the recent works of Ilegbusi *et al.* (1996, 1997), by studying numerically, the effects of valve on interface evolution and flow characteristics, over a range of Grashof number and Atwood number. A two-fluid model is employed to calculate the zone-averaged velocities and volume fraction of the fluids. The calculated volume fraction coupled with the interface evolution, provides a measure of the degree of mixing in the cavity. The mixing process is also examined from a dynamical system viewpoint in which the non-linear behavior of the flow field is analyzed in terms of its phase space trajectory and power spectrum.

This paper is divided into four sections of which this introduction is the first. In the next section, the mathematical formulation is presented comprising the governing equations, boundary and initial conditions and the numerical method. The computed results are presented and discussed in the next section. The last section contains the concluding remark that summarizes the major findings of this study.

2. FORMULATION

We consider two fluids which initially meet at a sharp density interface and separated by a thin plate (valve) with the heavier fluid on the left of a two-dimensional cavity, as shown in figure 1. The two fluids are assumed to be miscible and surface tension is neglected. After removing the valve vertically upwards, the fluids mix under the combined effects of buoyancy forces and kinetic energy induced by the valve. Under these conditions, the mixing process will be characterized by the valve removal velocity and the following three dimensionless numbers (Duval 1992)

$$\text{Atwood number:} \quad A_t \equiv \Delta\rho/(\rho_1 + \rho_2),$$

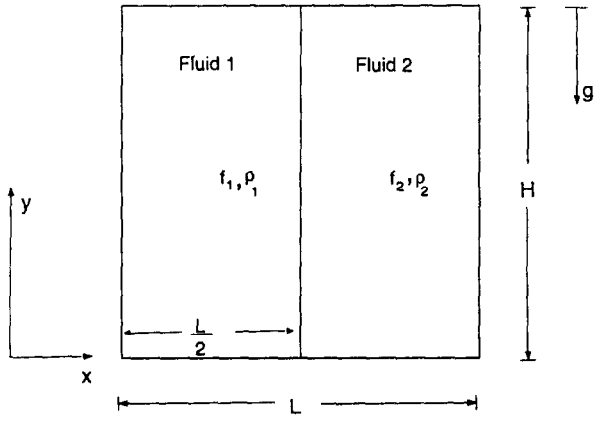

Figure 1. Initial positions of two fluids separate with a valve.

Table 1. Summary of cases considered

Case number	Gr	A_t	V_{val} (m/s)
1	3.7×10^5	5×10^{-5}	—
2	3.7×10^5	5×10^{-5}	0.025
3	3.7×10^5	5×10^{-5}	0.05
4	3.7×10^5	5×10^{-5}	0.1
5	3.7×10^5	0.13	0.05
6	3.7×10^5	0.33	0.05
7	1.45×10^4	5×10^{-5}	0.05
8	0.37	5×10^{-5}	0.05

$$\text{Aspect ratio:} \quad A_r \equiv H/L,$$

$$\text{Grashof number:} \quad \text{Gr} \equiv A_t g H^3/\nu^2,$$

where ρ_1 and ρ_2 represent density of the first and second fluid respectively, $\Delta\rho$ denotes the density difference, g is the gravity, H and L are the height and length of the cavity respectively and ν is the mean kinematic viscosity of the fluids. We consider a system with $A_r = 1$ and varying A_t, Gr and valve speed.

To quantify the mixing, a two-fluid model is employed (Spalding 1984; Ilegbusi *et al.* 1996, 1997). In this model the two fluids are regarded as two intermingled phases that are separated by sharp flexible boundaries that interact with each other through the sharing of space and pressure and exchange of mass and momentum. Thus at any location, there is a pair each of velocity components and volume fraction. The fluids share space in proportion to their existence probabilities or volume fractions f_1 and f_2, such that

$$f_1 + f_2 = 1. \tag{1}$$

In the above and subsequent equations, subscripts 1 and 2 represent the first and second fluid, respectively.

The governing transport equations expressing the conservation of mass and momentum for the two-fluid model under isothermal conditions are

Mass conservation

$$\frac{\partial(f_i\rho_i)}{\partial t} + \frac{\partial(f_i\rho_i u_i)}{\partial x} + \frac{\partial(f_i\rho_i v_i)}{\partial y} = 0 \tag{2}$$

Momentum (x-direction)

$$\frac{\partial(f_i\rho_i u_i)}{\partial t} + \frac{\partial(f_i\rho u_i^2)}{\partial x} + \frac{\partial(f_i(\rho_i u_i v_i)}{\partial y}$$

$$= -f_i\frac{\partial p}{\partial x} + F_i(u_1 - u_2) + f_i B_{i,x}$$

$$+ f_i\mu_i\left(\frac{\partial^2 u_i}{\partial x^2} + \frac{\partial^2 u_i}{\partial y^2}\right) \tag{3}$$

Momentum (y-direction)

$$\frac{\partial(f_i\rho_i v_i)}{\partial t} + \frac{\partial(f_i\rho_i v_i u_i)}{\partial x} + \frac{\partial(f_i\rho_i v_i^2)}{\partial y}$$

$$= -f_i\frac{\partial p}{\partial y} + F_i(v_1 - v_2) + f_i B_{i,y}$$

$$+ f_i\mu_i\left(\frac{\partial^2 v_i}{\partial x^2} + \frac{\partial^2 v_i}{\partial y^2}\right). \tag{4}$$

Table 2. Grid independence result at $t = 30$ s

Grid size	20 × 20	30 × 30	40 × 40	50 × 50	60 × 60
$f_1(L/4, H/4)$	0.2575	0.2237	0.2182	0.2158	0.2135

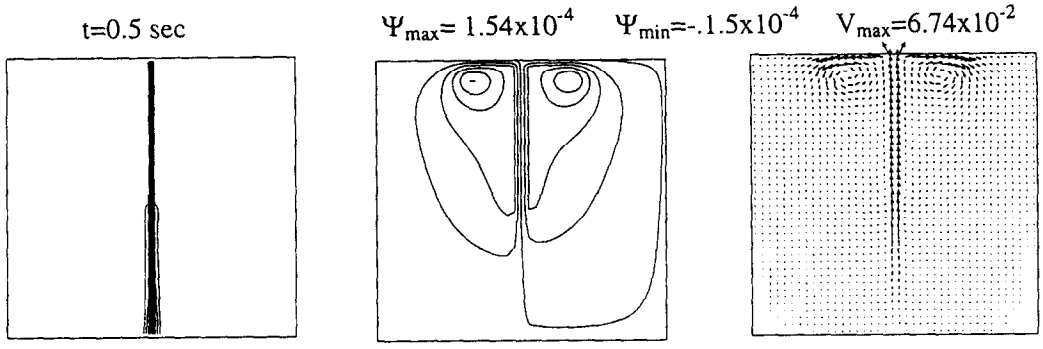

Figure 2. Interface behavior and flow pattern at $t = 0.5$ s for valve speed of 0.05 m/s.

In [2]–[4], the subscript i represents fluid i, u and v represents velocity components in x and y directions respectively, p is the shared pressure, and μ is the viscosity. The second term on the right of each momentum equation is an inter-fluid exchange term due to friction at the interface of the fluids, F is the interface friction coefficient and B is the volumetric body force. The interface friction coefficient is here expressed as

$$F_1 = -F_2 = c_d \tilde{\rho} f_1 f_2, \tag{5}$$

where $c_d = 20.0$ is an empirical constant (Ilegbusi *et al.* 1996, 1997) and, $\tilde{\rho}$ is the mixture density calculated from the relation

$$\tilde{\rho} = f_1 \rho_1 + f_2 \rho_2. \tag{6}$$

Initial and boundary conditions

The two fluids are initially at rest and separated by thin valve. The initial conditions are, therefore $t < 0$:

$$0 \leqslant x \leqslant L; 0 \leqslant y \leqslant H: \quad u_1 = u_2 = v_1 = v_2 = 0 \tag{7}$$

$$x < L/2; 0 \leqslant y \leqslant H: \quad f_1 = 1.0; f_2 = 0.0 \tag{8}$$

$$x \geqslant L/2; 0 \leqslant y \leqslant H: \quad f_1 = 0.0; f_2 = 1.0. \tag{9}$$

The boundary walls are fixed and no-slip conditions are imposed on all velocities parallel to the wall. The valve is considered a time-dependent boundary wall and the velocity components on it are expressed thus
$x = L/2$; $V_{val} t \leqslant y \leqslant H$:

$$v_1 = v_2 = V_{val} \tag{10}$$

$$u_1 = u_2 = 0, \tag{11}$$

where V_{val} is the valve removal velocity. The length of the valve (d_{val}) inside the cavity at time t is calculated from the relation

$$d_{val} = H - V_{val} t. \tag{12}$$

The values of parameters used in the calculations are summarized in table 1.

Mixing characteristics

Energy balance. The energy required for mixing is supplied by the potential energy of the system and the kinetic energy resulting from perturbation induced by the valve. The potential energy E_p at time t can be expressed as (Linden and Redondo 1991)

$$E_p = \int_0^L \int_0^H (\bar{\rho} - \rho_2) g \, \mathrm{d}\, h \, \mathrm{d}l, \qquad [13]$$

where $\bar{\rho}$ is the mixture density, ρ_2 is the density of the lighter fluid, and g is the gravity. Using [13] the maximum potential energy of the system which corresponds to the energy at the initial state can be calculated from the expression

$$E_{P_{max}} = \frac{gH^2L}{4}(\rho_1 - \rho_2). \qquad [14]$$

The kinetic energy of the system can be calculated from the relation

$$E_K = \int_0^v mv \, \mathrm{d}\, v, \qquad [15]$$

where m is the mass of the fluid mixture, and v is the velocity. The valve motion introduces an additional kinetic energy which may be very significant at high valve speeds. In order to account for this effect, the kinetic energy contributed by the valve motion is here expressed as

$$E_{Kv} = \int_0^{t_{rm}} \int_0^L \int_0^H mv\left(\frac{\partial v}{\partial x}\,\mathrm{d}x + \frac{\partial v}{\partial y}\,\mathrm{d}y + \frac{\partial v}{\partial t}\,\mathrm{d}t\right) \qquad [16]$$

where t_{rm} is the total travel time of the valve within the cavity. Although [16] includes contribution from the potential energy, the latter contribution is relatively small within the time t_{rm} as will be shown in the presentation of results. The maximum energy can thus be estimated as the sum of the initial potential energy and the total kinetic energy induced by the valve removal process. The system will have minimum energy if all potential and kinetic energies can be dissipated without mixing. Under such situation, the fluids will be stably stratified with the lighter fluid overlying the heavier fluid. The minimum energy is thus equal to the minimum potential energy which can be obtained from [13] of the form

$$E_{min} = Ep_{min} = \frac{gH^2L}{8}(\rho_1 - \rho_2). \qquad [17]$$

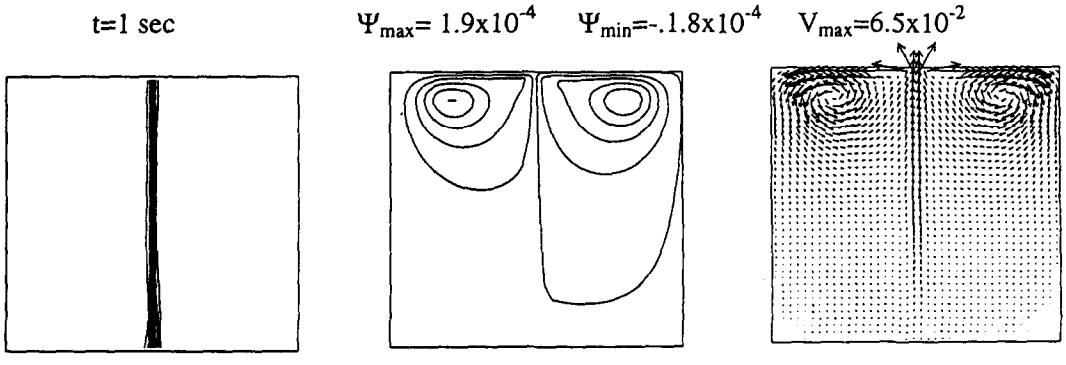

Figure 3. Interface behavior and flow pattern at $t = 1$ s for valve speed of 0.05 m/s.

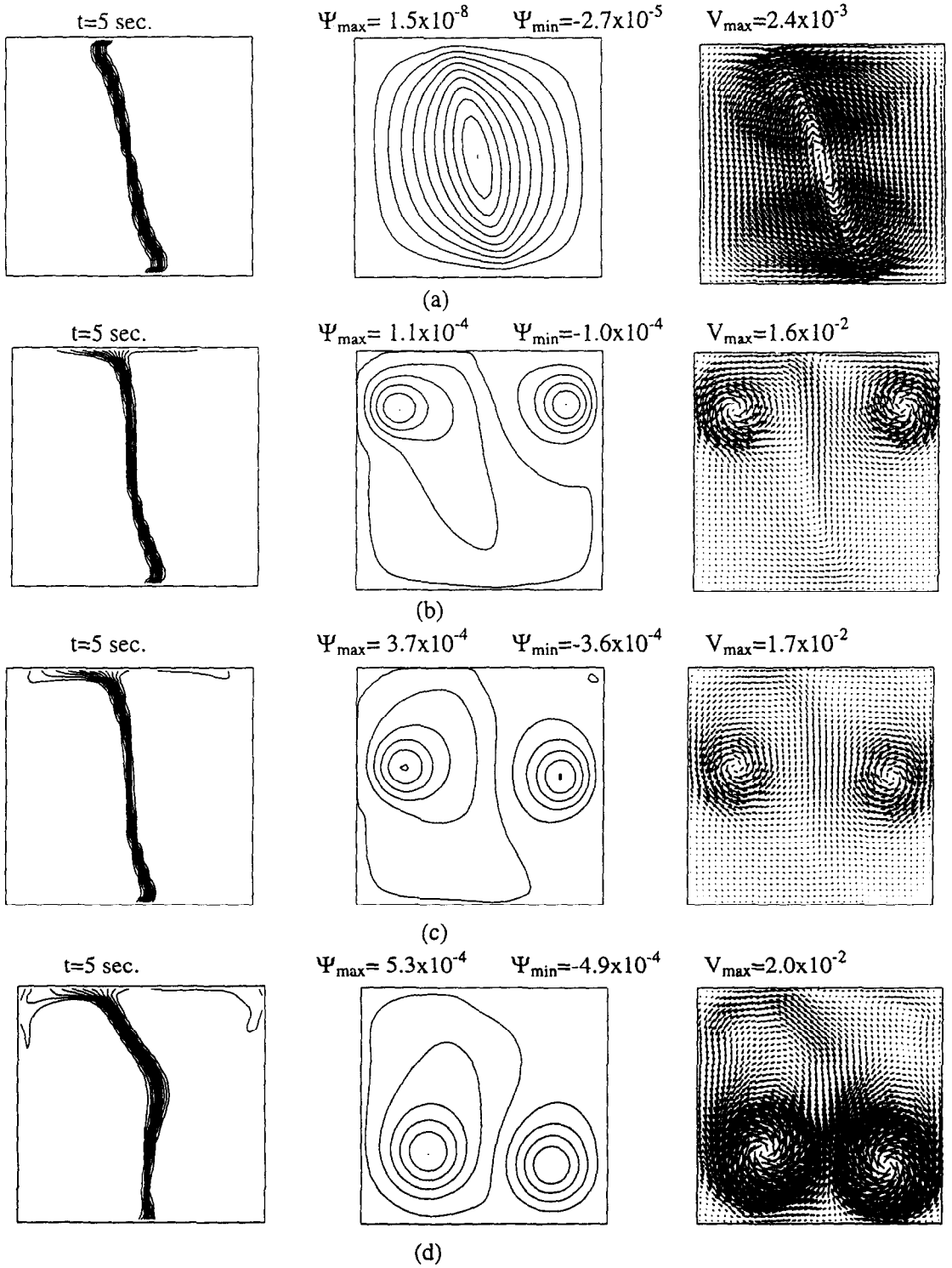

Figure 4. Interface behavior and flow pattern: (a) no valve; (b) V_{val} = 0.025 m/s; (c) V_{val} = 0.05 m/s; (d) V_{val} = 0.1 m/s.

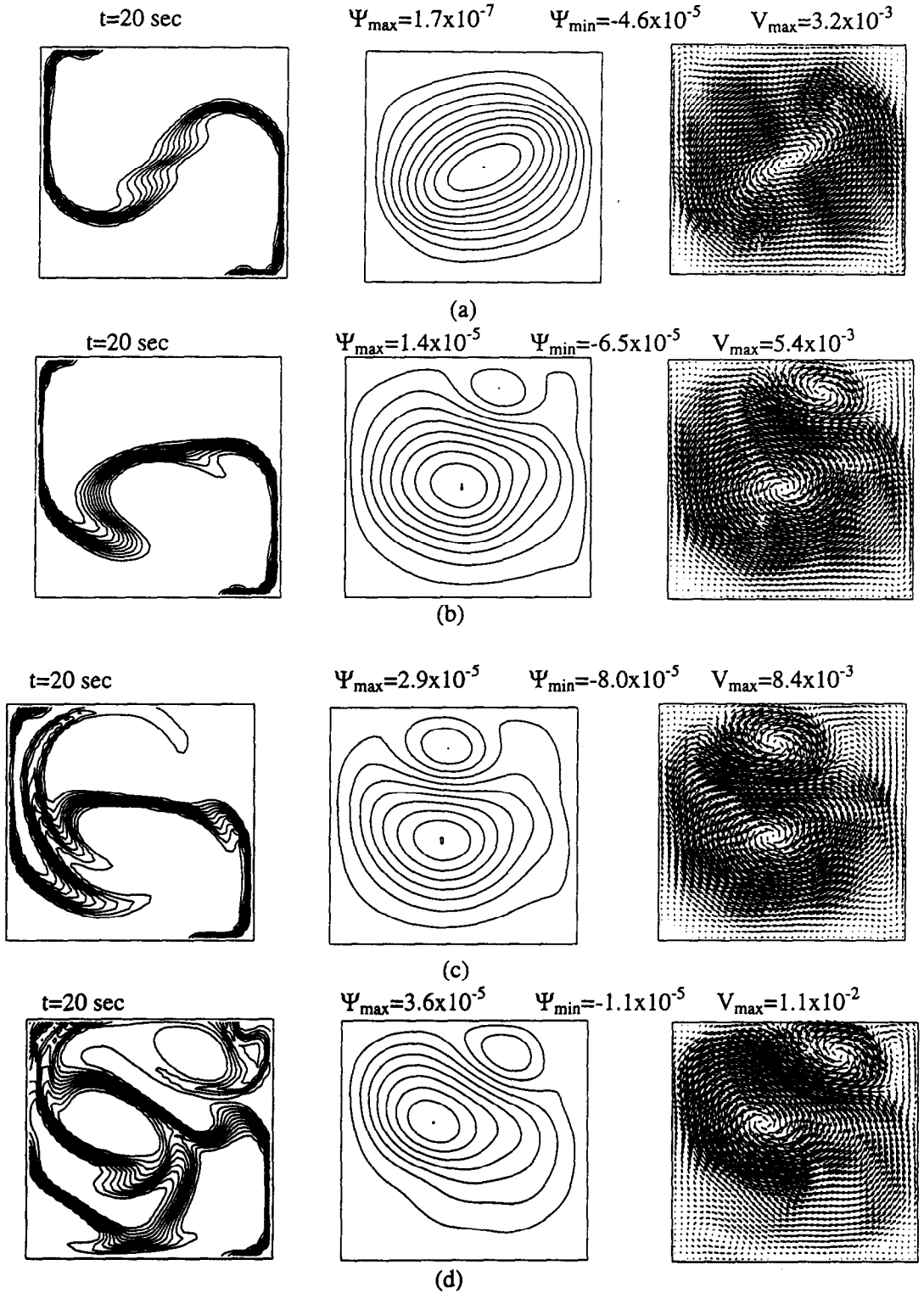

Figure 5. Interface behavior and flow pattern: (a) no valve; (b) $V_{val} = 0.025$ m/s; (c) $V_{val} = 0.05$ m/s; (d) $V_{val} = 0.1$ m/s.

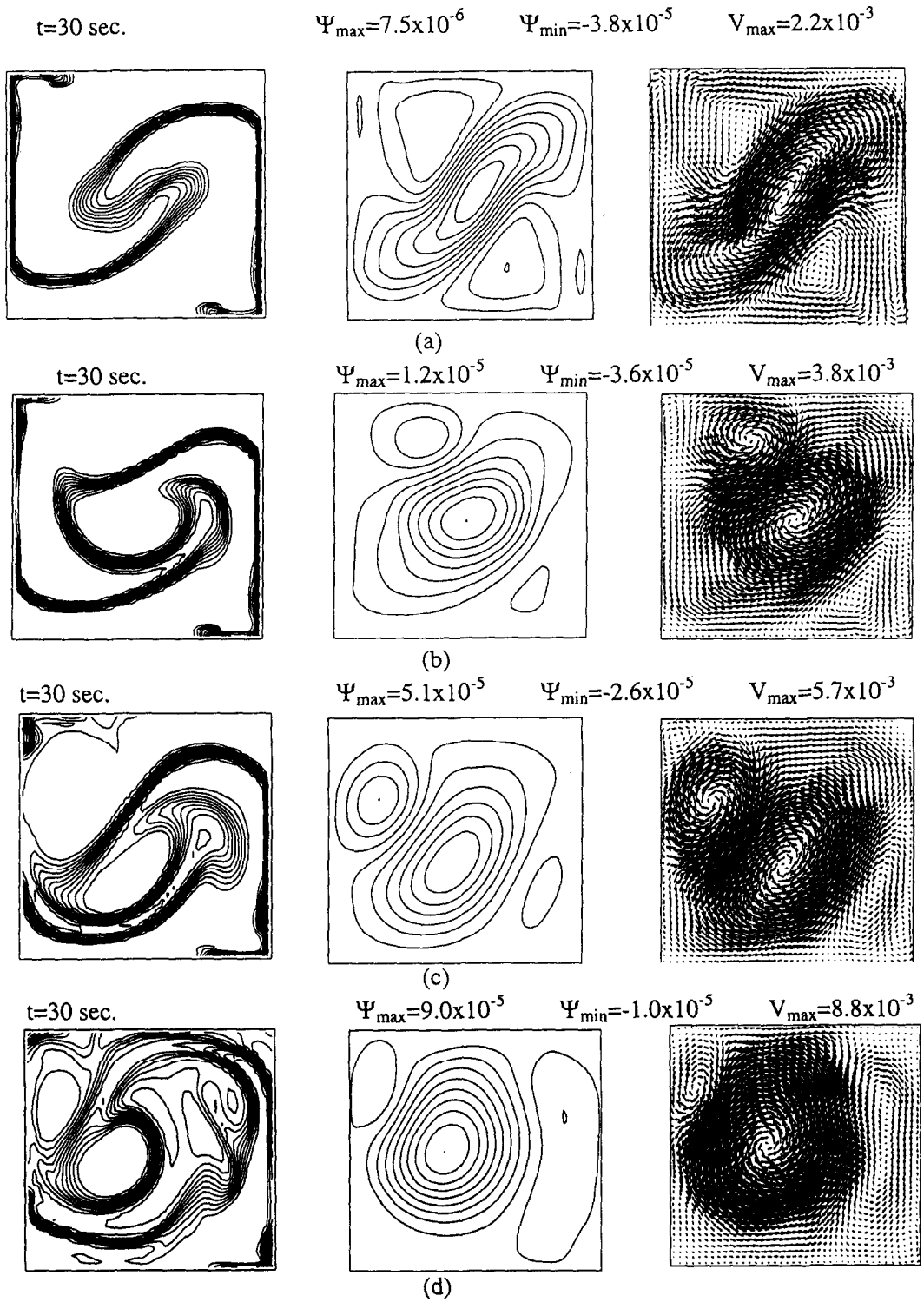

Figure 6. Interface behavior and flow pattern: (a) no valve; (b) $V_{val} = 0.025$ m/s; (c) $V_{val} = 0.05$ m/s; (d) $V_{val} = 0.1$ m/s.

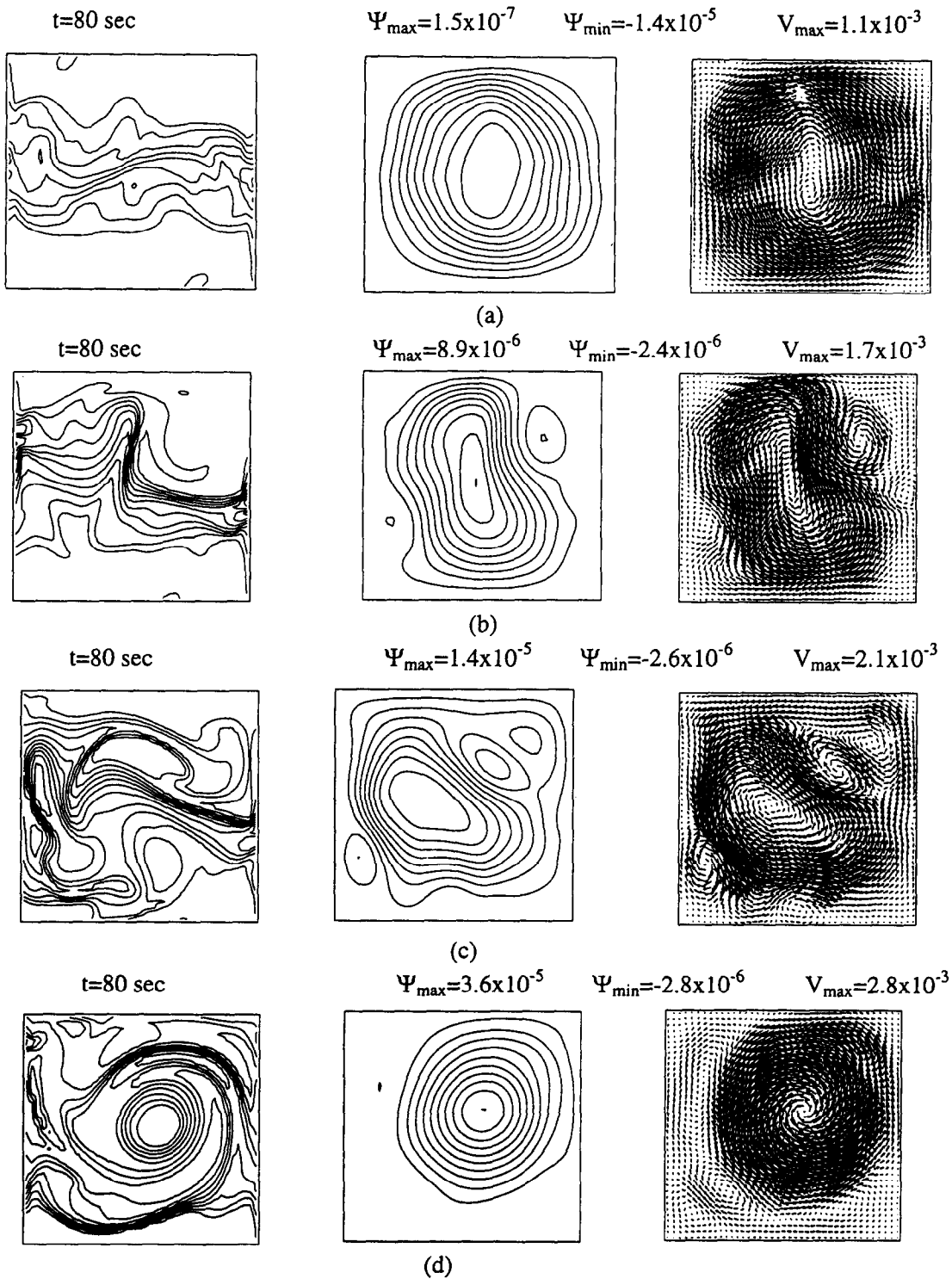

Figure 7. Interface behavior and flow pattern: (a) no valve; (b) $V_{val} = 0.025$ m/s; (c) $V_{val} = 0.05$ m/s; (d) $V_{val} = 0.1$ m/s.

Mixing efficiency. We define efficiency for the system as the ratio of the energy used to mix the fluids to the energy lost due to viscous dissipation. Following Linden and Redondo (1991), the mixing efficiency can be expressed as

$$\eta = \frac{E - E_{\min}}{E_{\max} - E_{\min}}, \qquad [18]$$

where E is the total energy of the system when mixing by convection is completed, and $E_{\min}$ and $E_{\max}$ represent the minimum and maximum energy of the system, respectively.

Interface elongation and width. The following two additional parameters are used to quantify the state of mixing inside the cavity (Ilegbusi *et al.* 1996, 1997):

(i) dimensionless length l^* defined as

$$l^* = \frac{l - l_0}{l_0}, \qquad [19]$$

where l_0 and l represent the interface length at initial and a later time t, respectively. The latter is calculated from the expression (Ottino *et al.* 1979)

$$l(t) = \int_{l_0}^{l} \exp\left\{ \int_0^t D(l, t):\mathbf{n}(\underline{l}_0, t_0)\, \mathrm{d}t \right\} \mathrm{d}l, \qquad [20]$$

where D is the symmetric part of the viscous stress tensor, and $\mathbf{n}$ is the unit vector;

(ii) dimensionless width w^*, expressed as

$$w^* = \frac{w - w_0}{w_0}, \qquad [21]$$

where w is the interface width, defined as the average distance between the 0.05 and 0.95 contours of the volume fraction of one fluid at time t, and w_0 is the initial width.

The characteristic time of the mixing process is non-dimensionalized with the kinematic time scale T_k defined as a function of the Atwood number given by (Ilegbusi *et al.* 1977)

$$T_k = \left(\frac{H}{gA_t}\right)^{1/2}. \qquad [22]$$

Numerical details

The coupled nonlinear set of equations [1]–[4] is solved by a finite-domain numerical technique (Patankar and Spalding 1972). The conventional upwind schemes often employed for discretizing the convection terms in the governing equations are known to cause numerical diffusion which produce unphysical results. Although this problem can be reduced by use of a high-order scheme, numerical oscillation may occur due to the steep density gradient in the present problem. Thus the Van–Leer Scheme (Andrews 1995) has been employed in the computation of the convective terms to eliminate the numerical oscillation while maintaining a high-order accuracy.

The equations are solved by a fractional time step-technique in which at each time step, an advection and calculation is performed followed by a Lagrangian source term update. A Poisson equation is obtained for the pressure by substituting updated velocities with correction terms into the continuity equation. The Poisson equation is then solved using Gauss–Seidel iteration method that ensures that new velocities and pressures satisfy the continuity and momentum equations. The details of the method can be found in Andrews (1995) and Ilegbusi *et al.* (1996, 1997).

A numerically accurate result is obtained in each case with a 40 × 40 grid system and 0.01 second time step. This grid number has been selected form a systematic grid refinement test performed on 20 × 20, 40 × 40, and 60 × 60 grid systems. The result of this test at a typical time (t = 30 s) are presented in table 2. It is seen that the volume fraction of fluid 1 (f_1) at a location ($L/4$, $H/4$) does not change significantly beyond the 40 × 40 grid structure. The observed trend in f_1 values is typical of other locations in the system.

3. RESULTS

The system considered is characterized primarily by the Grashof number, Atwood number and valve speed. The effects of these parameters on the mixing characteristics are presented here. The interface is identified by the interval between the 0.1 and 0.9 contour values of the volume fraction of one of the fluids. The flow field is represented by the plots of the velocity vectors and streamlines.

Effect of valve speed

The results showing the effect of valve speed on flow behavior and mixing are presented in figures 2–8. The calculations are performed at a constant Grashof number $Gr = 3.7 \times 10^5$ for three valve speeds, 0.025, 0.05 and 0.1 m/s, in addition to a situation without valve. The latter case corresponds to instantaneous valve removal without perturbation. The valve acts as a time-dependent boundary wall which affects the mixing characteristics of the system.

Figure 2 presents the result when the valve is half open (i.e. $t = 0.5$ s) for a valve speed of 0.05 m/s. The fluid particles adjacent to the valve accelerate upward toward the upper wall due

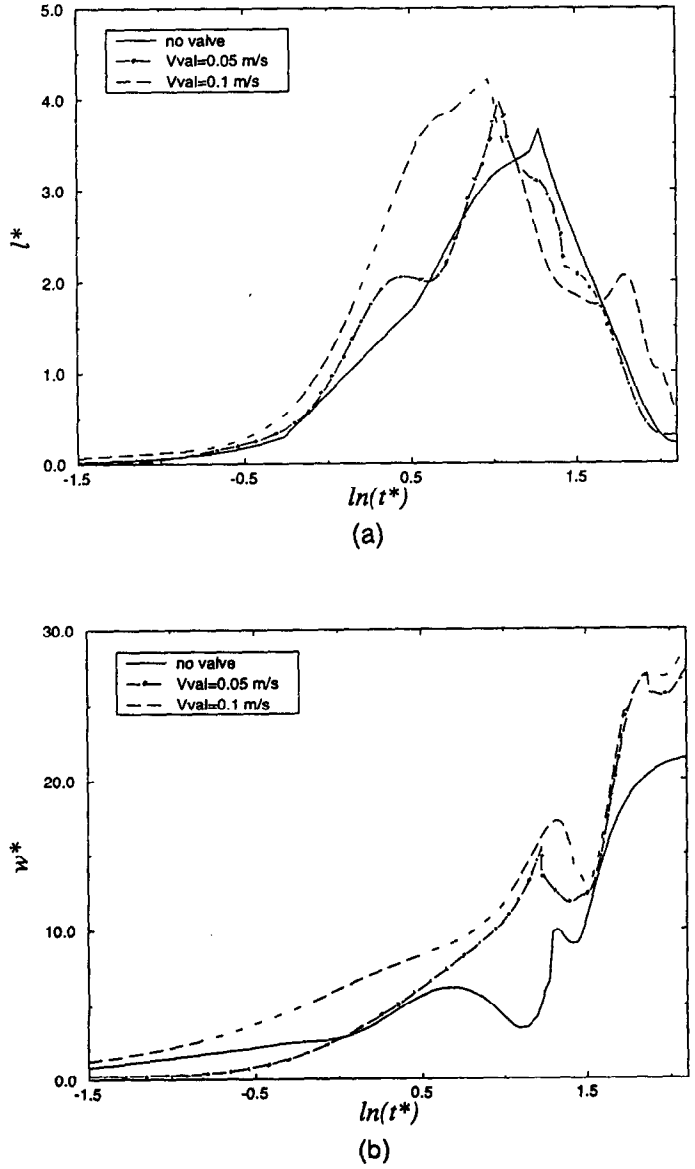

Figure 8. Valve effect on the interface: (a) elongation; (b) width.

to the no-slip condition. The fluid subsequently changes direction, forming two vortices which rotate in opposite directions at the top of the cavity. The interface behavior and velocity field at $t = 1$ s are shown in figure 3. The valve is now fully open and the vortices continue to move in opposite directions in the cavity. The interface is seen to be slightly distorted by the wake behind the valve.

Figure 4 compares the flow field and interface profiles after 5 s in the absence of valve (figure 4(a)) and three valve speeds 0.025, 0.05 and 0.1 m/s. Figure 4(a) shows that in the absence of valve, the interface is pushed symmetrically from the top and bottom of the cavity as a result of unbalanced pressure forces. In contrast, figure 4(b)–(d) show that the valve introduces initial perturbation and additional kinetic energy to the system. These figures show that the effects of the inherent potential energy of the system and the added kinetic energy are generally comparable, though the relative magnitudes depend on the Grashof number and valve speed. A small mixing region develops at the top of the cavity due to perturbation introduced by the valve, leading to expansion of the interface. As valve speed increases the interface at this region accelerates towards both sides of the cavity due to the increased perturbation. However, the interface breaks up faster at the right of the cavity due to the larger buoyancy force. The interface area is larger and the vortex is stronger on the left part of the cavity due to inertia effect. Two counter-rotating vortices are formed which progressively move towards the bottom surface as the valve speed increases. Figure 4(d) shows that these counter-rotating vortices keep the interface stationary at the higher valve speed. Figure 4(a)–(d) also show that the perturbation at the center of the cavity increases with the valve speed.

The effect of valve speed at a later time $t = 20$ s is presented in figure 5. Figure 5(a) shows that in the absence of the valve, the interface deforms to an internal wave as the light fluid overlies the heavier fluid. A perturbation at the core region is apparent at this stage resulting from Kelvin–Helmholtz instability which develops due to the relative motion of the two fluids. Figure 5(b) shows that the internal wave loses its sinusoidal shape even at a relatively low valve speed. As the valve speed increases, a counter-clockwise circulation is replaced by two vortices rotating in opposite directions. The strength of the upper vortex increases with valve speed and

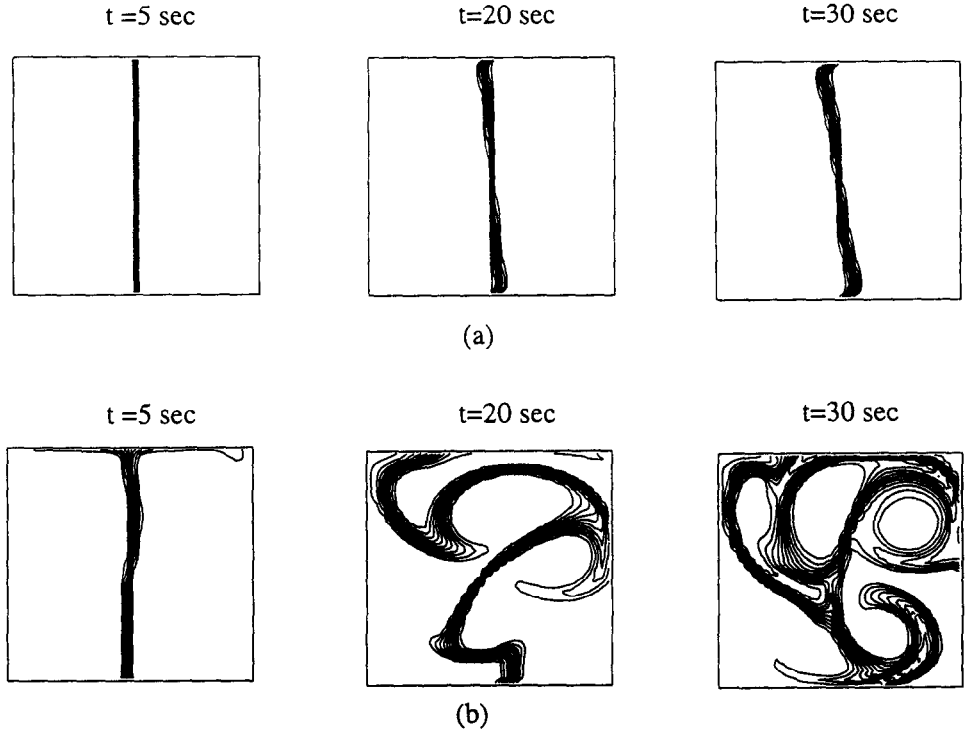

Figure 9. Effect of valve on interface evolution at an intermediate Grashof number (Gr = 1.45×10^4, $A_t = 5 \times 10^{-5}$): (a) no valve; (b) $V_{val} = 0.05$ m/s.

the interface is dragged towards the upper part of the cavity. It is also seen that the interface rolls and breaks up from several locations at high valve speeds.

The corresponding results after 30 s are presented in figure 6. Figure 6(a) shows that the interface exhibits a 'tendril' structure which develops from growth of the Kelvin–Helmholtz instability for the case without a valve. This structure is still apparent at low valve speed (figure 6(b)). The interface breaks-up at intermediate valve speed and the flow field is replaced by a vortex at the center (figure 6(c)). As seen in figure 6(d) the tendril structure disappears t high valve speed, and mixing occurs over a relatively wide region.

The late time behavior of the system at $t = 80$ s is presented in figure 7. In the case without a valve (figure 7(a)), the two fluids are now stably stratified and further mixing takes place by diffusion. Wall plumes that were formed at top and bottom parts of the cavity dissipate in the flow field as a result of convective and diffusive effects. At low valve speed (figure 7(b)), the two fluids are stably stratified although convection is still important, resulting in a slight oscillation of the interface. At intermediate and high valve speeds (figure 7(c), (d)), it is seen that the kinetic energy of the system has not completely decayed and the mixing region is relatively large. After all the kinetic energy is subsequently dissipated, diffusion ensues until complete mixing of the fluids.

The time evolution of interface elongation and mixing width are presented in figure 8. It is seen that the interface elongates exponentially to a peak value until breakup. This exponential increase indicates that the system exhibits chaotic behavior (Ottino 1989). Figure 8(a) shows that while the maximum value of the interface length is not significantly affected by the valve speed, the approach to this maximum is faster as valve speed increases. On the other hand, figure 8(b) shows that the interface (mixing) width increases significantly with the valve speed. This trend can be attributed to the increased kinetic energy induced by the valve.

Effect of Grashof number

The results showing effect of Grashof number on flow behavior are presented in figures 9 and 10 coupled with those presented earlier in figures 2–8. The Grashof number is varied in the laminar

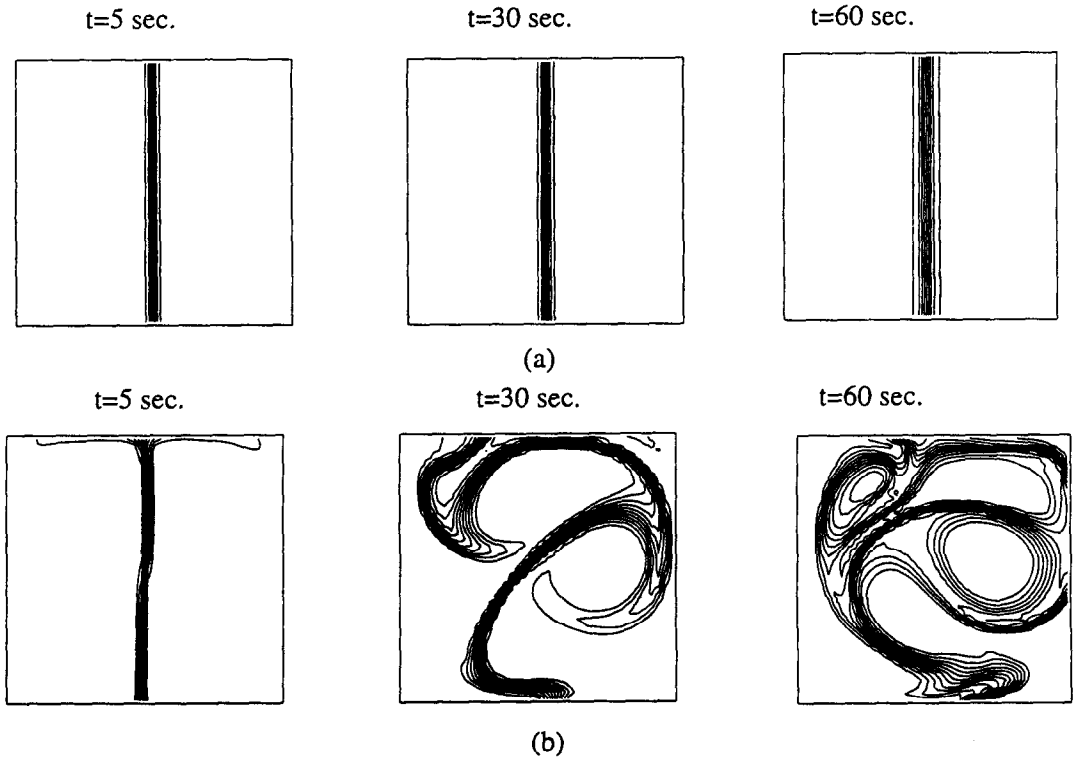

Figure 10. Effect of valve on interface evolution at low Grashof number (Gr = 0.37, $A_t = 5 \times 10^{-5}$): (a) no valve; (b) $V_{val} = 0.05$ m/s.

regime from $1 \leqslant Gr \leqslant 10^5$ at a specific valve speed of 0.05 m/s. The results presented in figures 2–8 for a high Grashof number ($Gr = 3.7 \times 10^5$) and valve speed of 0.05 m/s have shown that the kinetic energy introduced to the system by the valve and the buoyancy forces generated by the potential energy have comparable effects. Figure 9 shows the corresponding interface behavior and flow field at an intermediate Grashof number ($Gr = 1.45 \times 10^4$). It is seen that the results at the early stages are essentially similar to those at high Grashof number presented in figures 2–8. At a later stage, the valve effect is essentially superimposed on the mixing. Since the buoyancy forces are lower in figure 9, than in figures 2–8, the results indicate that the kinetic energy introduced by the valve significantly influences the mixing characteristics. This trend is confirmed in figure 10, which shows that the valve speed plays an increasingly dominant role in the mixing process as Grashof number decreases.

Effect of Atwood number

The effect of Atwood number on the interface evolution and flow behavior are presented in figures 11–13. The Grashof number and valve speed are chosen as 3.7×10^5 and 0.05 m/s, respectively, and the Atwood number is varied without the range $5 \times 10^{-2} \leqslant A_t \leqslant 0.33$. The result after 5 s for $A_t = 0.11$ and 0.33 are shown in figure 11. It is seen that the velocity field is larger at the left side of the cavity containing the heavy fluid, as Atwood number increases, due to the inertia gained during the valve-removal process. The flow field pushes the interface from the top and bottom parts of the cavity. The interface propagates faster at the bottom surface as Atwood number increases and folds on itself at the highest Atwood number considered. It is also seen that the vortex on the left part reaches the bottom of the cavity at the highest Atwood number. Figure 12 shows that after about 20 s, the interface evolves as a result of subsequent motion and an overturning of the interface is apparent for all cases considered. It is interesting that distortion of the interface due to Kelvin–Helmholtz instability occurs at the left side rather than the center of the cavity in contrast to the result reported by Ilegbusi *et al.* (1996), in the absence of valve. It is seen that the interface is also partially dragged towards the upper part of the cavity at the lower Atwood number. Figure 13 shows that the interface breaks up before $t = 30$ s, leading to a wider mixing region. It is significant that the whorl and tendril interface structures reported by Ilegbusi

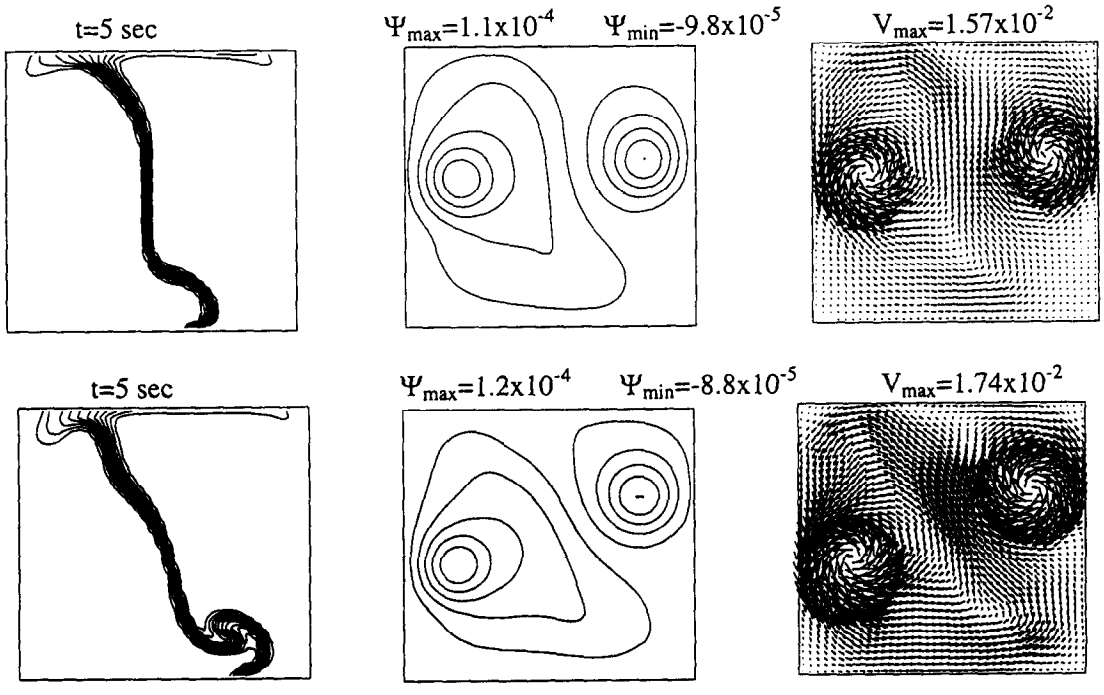

Figure 11. Effect of Atwood number on interface evolution and flow behavior at $t = 5$ s ($Gr = 3.7 \times 10^5$, $V_{val} = 0.05$ m/s): (a) $A_t = 0.13$; (b) $A_t = 0.33$.

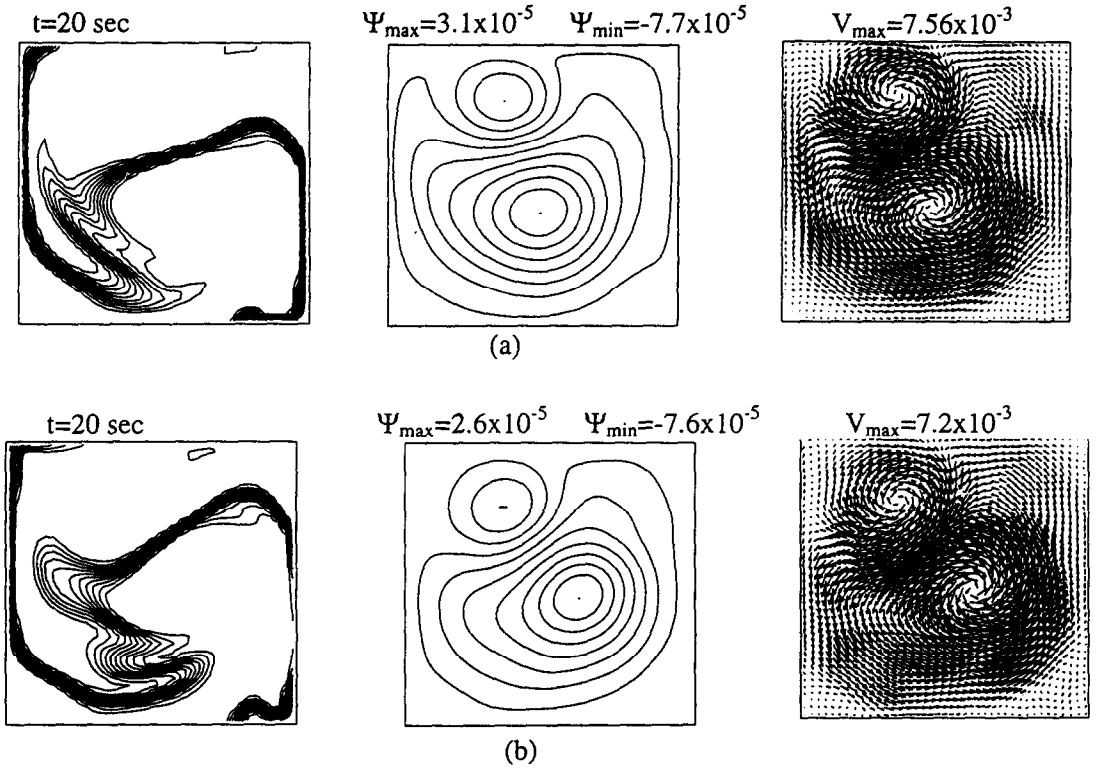

Figure 12. Effect of Atwood number on interface evolution and flow behavior at $t = 20$ s ($Gr = 3.7 \times 10^5$, $V_{val} = 0.05$ m/s): (a) $A_t = 0.13$; (b) $A_t = 0.33$.

et al. (1996, 1997), at relatively high Grashof numbers in the absence of valve are not evident in the present situation.

Energy balance

Figure 14 illustrates the energy balance for the system in the absence of valve. It is seen that the potential energy of the system decreases very rapidly at the early stage of the mixing process and subsequently approaches a constant value. However, it should be noted that the decay of potential energy in the initial 2 s (which corresponds to the longest valve residence time for the cases to be considered) is relatively small. The kinetic energy rises to a peak value before the time ($t = 30$ s) corresponding to the breakup of the interface. This energy subsequently decays due to viscous dissipation and wall shear stresses. At this stage, the system becomes stably stratified (see figure 7) and flow oscillation stops.

Figure 15(a), (b) depict the corresponding energy balance for the system for the various valve speeds considered. Figure 15(a) shows that the additional kinetic energy induced by the valve increases with valve speed. The effect of this kinetic energy and that resulting from the potential energy of the system are generally additive. It is seen that both kinetic energy components dissipate very rapidly. Figure 15(b) shows that at the late time, the potential energy of the system increases with the valve speed, indicating that the kinetic energy induced by the valve increases the degree of mixing.

Mixing efficiency

Using [18], the theoretical maximum efficiency in the absence of valve is 1.0, compared with a value of 0.5 obtained for Rayleigh–Taylor instability by Linden and Rodendo (1991). The mixing efficiency of the system considered here is presented in figure 16 for a range of valve speeds. Only the efficiency of convective mixing is considered since the diffusive effect is relatively small and occurs at the end of the convective regime. Thus, a reference time $t = 80$ s has been chosen at which all the kinetic energy of the system with valve has been completely dissipated (see figure 7).

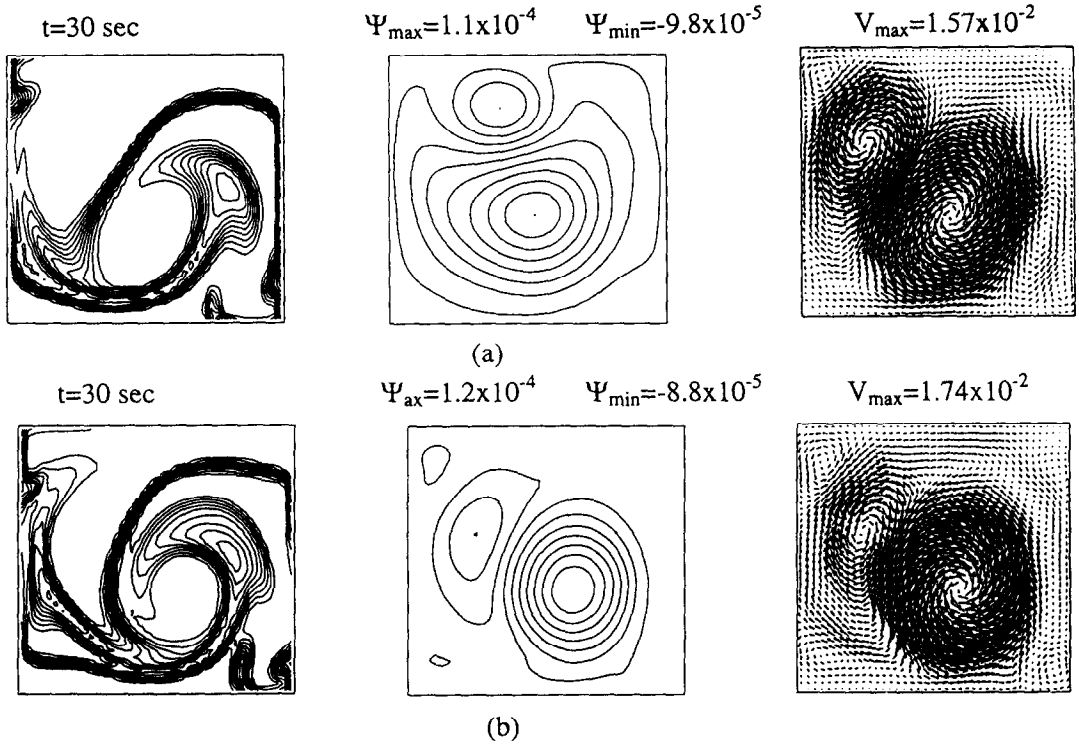

Figure 13. Effect of Atwood number on interface evolution and flow behavior at $t = 30$ s (Gr = 3.7×10^5, $V_{val} = 0.05$ m/s): (a) $A_t = 0.13$; (b) $A_t = 0.33$.

Figure 16 shows that the mixing efficiency is enhanced at low valve speed and reaches a peak value in the absence of valve. It is significant that figure 16 shows that the efficiency does not exceed 0.35 for all cases considered, which is comparable to the value of 0.34 obtained by Duval (1992) based on a different approach. However, it should be noted that if mixing efficiency is defined by

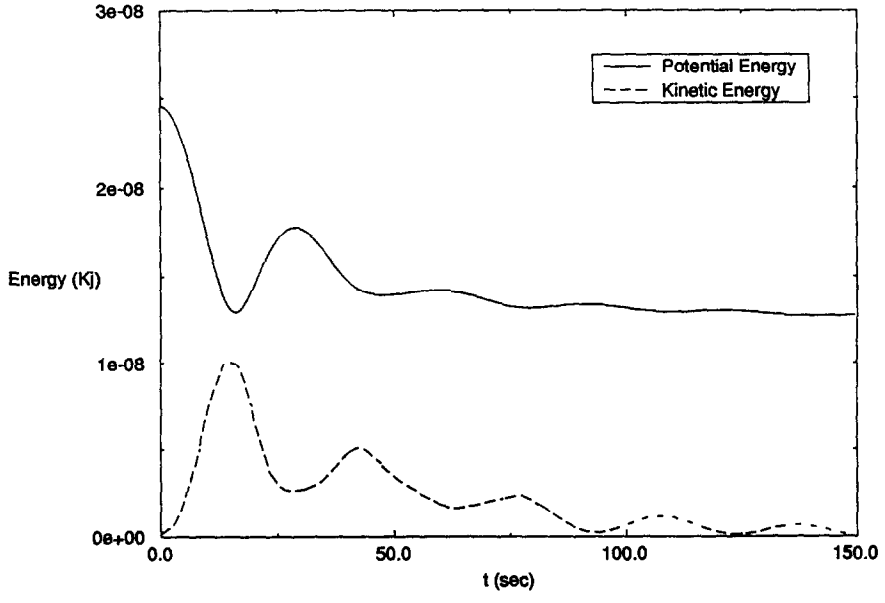

Figure 14. Energy balance in the absence of valve.

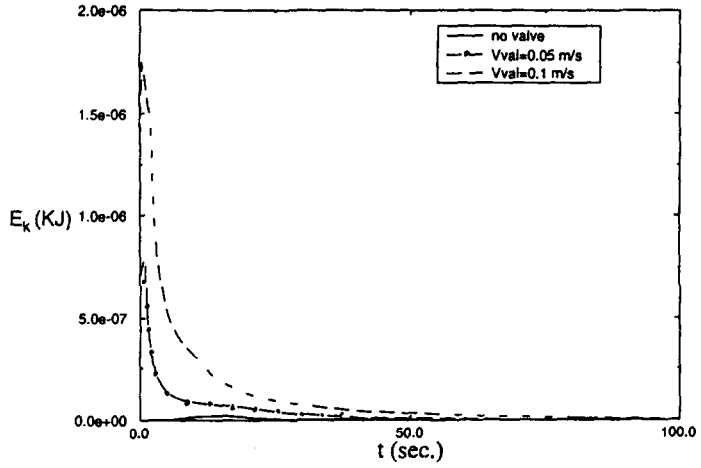

(a)

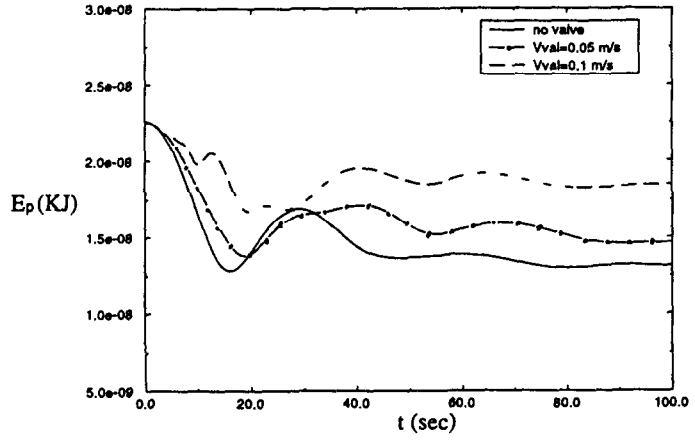

(b)

Figure 15. Energy balance in the presence of valve: (a) kinetic energy; (b) potential energy.

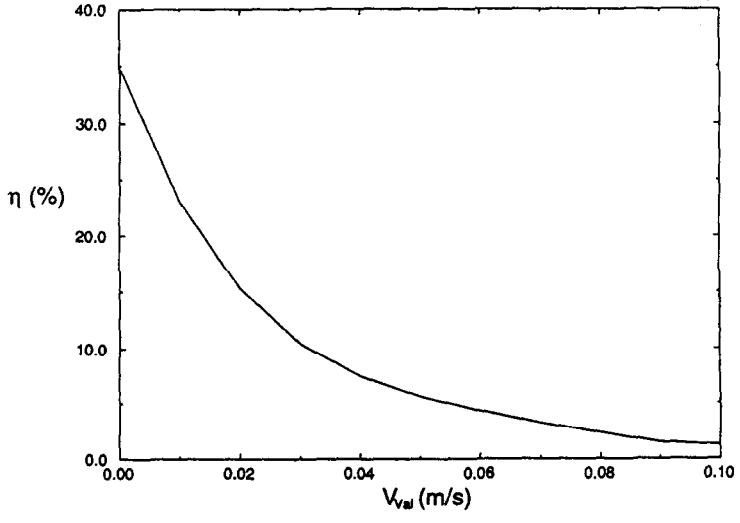

Figure 16. Mixing efficiency as a function of valve speed.

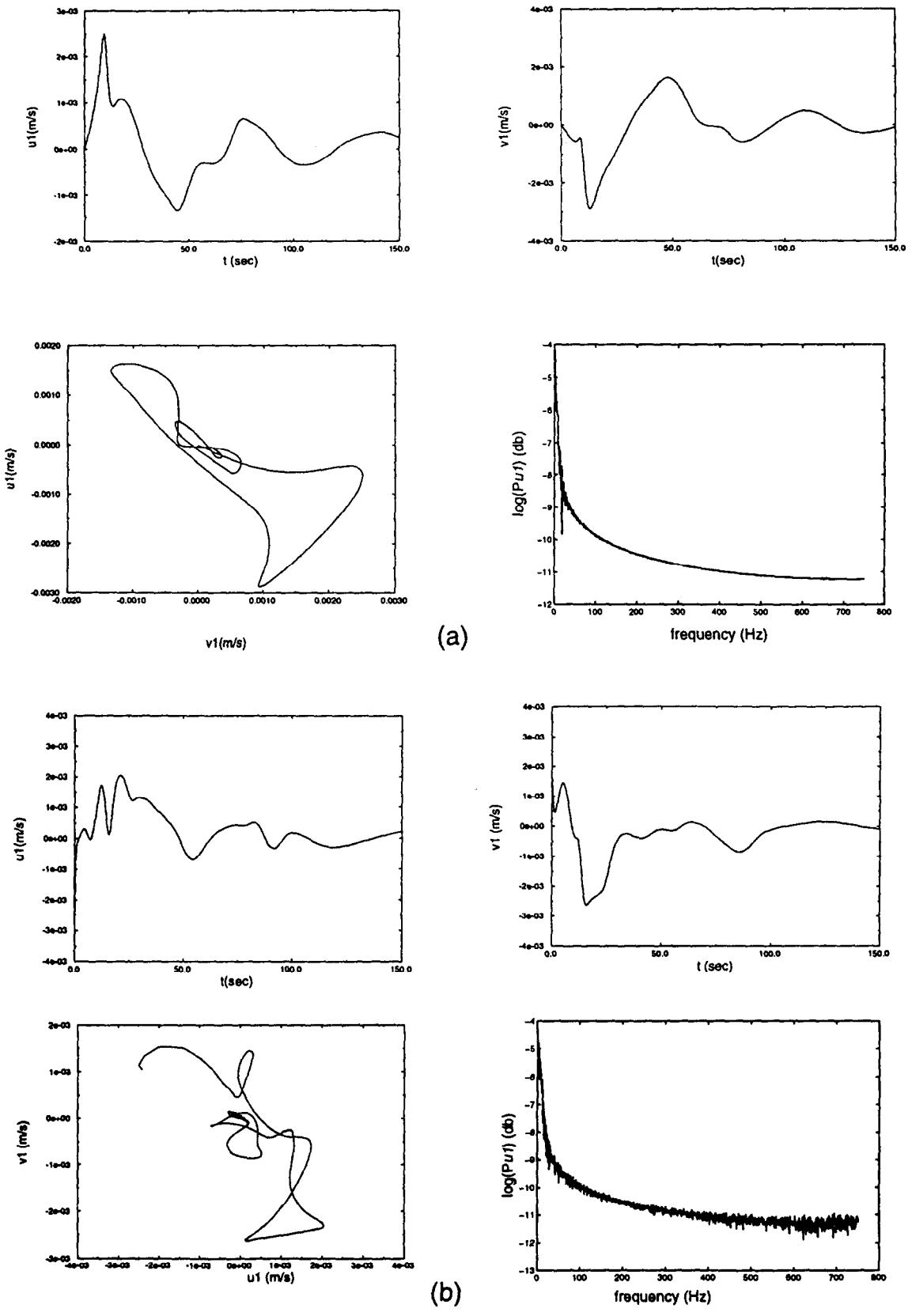

Figure 17. System dynamics of mixing at a fixed point ($L/4$, $H/4$, t) (Gr = 3.7×10^5, $A_t = 5 \times 10^{-5}$): (a) no valve; (b) $V_{val} = 0.1$ m/s.

Table 3. Influence areas of parameters considered

Properties	Valve speed	Gr	A_t
Identification of flow regimes	—	✓	✓
Interface structure and flow behavior	✓	✓	✓
Max. interface elongation	✓	✓	✓
Max. interface width	✓	✓	✓
Flow asymmetry	✓	—	✓
Mixing efficiency	✓	✓	✓
Initial perturbation	✓	—	—
Additional kinetic energy	✓	—	—

how well the fluids mix in a given time, the fastest valve speed is the most efficient since the mixing width spans the entire cavity after a relatively short time of about 30 s (see figure 6).

System dynamics

The governing equations presented earlier constitute a set of coupled non-linear partial differential equations that is relevant to non-linear dynamics. In the time-dependent domain, the dynamical behavior of the flow field can be represented using the phase trajectories and power spectrum. The phase trajectories and accompanying amplitudes of the u and v velocities are considered at a fixed point as a function of frequency. The fast fourier transformation (FFT) based on the standard Cooley–Tukey algorithm which is implemented in MATLAB mathematical code (Krauss *et al.* 1994) is employed for the calculations. A total of 1000 points are sampled for estimating the amplitudes in the frequency domain.

Figure 17 presents the system dynamics of the mixing process for a fixed point of the flow field at $(L/4, H/4, t)$ for two situations corresponding to the absence of valve and 0.1 m/s valve speed. The Grashof number and Atwood number are 3.7×10^5 and 5×10^{-5}, respectively. The time histories of the velocities clearly indicate that the flow field is aperiodic in both cases considered. The phase space trajectories are irregular, and have more intersections in the presence of the valve. The power spectrum plots for the system show that maximum power is concentrated at low frequencies in all cases. Such broadband and noisy spectra are characteristic of a chaotic motion (Brown and Smith 1990; Duval 1992). This chaotic behavior is also confirmed by the exponential increase of the interface length in figure 8(a).

4. CONCLUSION

The effects of valve removal on mixing of two fluids have been investigated with a two-fluid model over a range of Grashof numbers and Atwood numbers. The flow structure and interface behavior have been represented by the volume fractions of the fluids, velocity vectors and streamline patterns. The major findings of the study can be summarized as in table 3, showing how the various parameters investigated influence the flow characteristics.

The valve acts as a time-dependent boundary wall which affects the mixing characteristics of the system. It is shown that valve removal causes perturbation of the fluid interface and a more intense mixing than in the absence of valve. The kinetic energy introduced by the valve and the potential energy of the system are found to have comparable effects. Buoyancy forces play a dominant role on mixing at high Grashof numbers and low valve speeds, while valve effect is superimposed on mixing at low Grashof numbers. The mixing efficiency defined relative to the actual energy used for mixing however decreases as valve speed increases, but mixing is more rapid at the higher valve speed.

The interface evolves symmetrically at relatively low Atwood numbers in the absence of valve and becomes more asymmetric as valve speed increases. The Atwood number is also found to significantly influence the mixing. Folding and breakup of the interface occur quite rapidly due to the inertia gained by the fluids from the valve removal process. The 'tendril' and 'whorl' flow structures formed without valve are conspicuously non-existent in the presence of a valve.

The dynamical system characteristics at high Grashof numbers indicate that the flow field is aperiodic, the phase space trajectories display irregular patterns and the power spectrum concentrates at low frequencies, indicating chaotic mixing.

Acknowledgements—The authors would like to acknowledge the useful discussion with Dr M. J. Andrews, the financial support from Nigde University (Turkey) to one of the authors (M.D.M.), and the ALCOA Foundation Award.

REFERENCES

Andrews, M. J. and Spalding, D. B. (1990) A simple experiment to investigate two-dimensional mixing by Rayleigh–Taylor instability. *Phys. Fluids A* **2,** 922–924.

Andrews, M. J. (1995) Accurate computation of convective transport in transient two-phase flow. *International Journal for Numerical Methods in Fluids* **21,** 205–222.

Brown, M. G. and Kevin, B. S. (1991) Ocean stirring and chaotic low-order dynamics. *Phys. Fluids A* **3,** 1168–1192.

Duff, R. E., Harl, F. H. and Hirt, C. W. (1992) Effects of diffusion on interface instability between gases. *Phys. Fluids* **5,** 417–425.

Duval, W. M. B. (1992) Numerical study of mixing of two fluids under low gravity. NASA TM 105865.

Duval, W. M. B. (1992) The kinematics of buoyancy induced mixing. *Proceedings of the Eigth European Symposium on Materials and Fluid Sciences in Microgravity*, Universite Libre de Bruxelles, Belgium, 12–16 April.

Emmons, H. W., Chang, C. T. and Watson B. C. (1960) Taylor instability of finite surface waves. *J. Fluid Mech.* **7,** 177–193.

Ilegbusi, O. J., Mat. M. and Andrews, M. J. (1996) Effect of Atwood number on the kinematic mixing of two fluids. *J. of Material Processing and Manufacturing Science* **4,** 323–337.

Ilegbusi, O. J., Mat, M. and Andrews, M. J. (1997) The deformation and kinematic mixing of a collapsing interface. *Applied Mathematical Modelling* (accepted for publication).

Krauss, P. T., Shure, L. and Little, J. N. (1994) *Signal Processing Toolbox for Use with MATLAB*. The MathWorks, Inc., Natick, MA.

Linden, P. F. and Redondo, J. M. (1991) Molecular mixing in Rayleigh–Taylor instability. Part I: Global mixing. *Phys. Fluids A* **3,** 1269–1277.

Linden, P. F., Redondo, J. M. and Youngs, D. L. (1994) Molecular mixing in Rayleigh–Taylor instability. *J. Fluid Mech.* **265,** 97–124.

Lewis, D. J. (1950) The instability of liquid surfaces when accelerated in a direction perpendicular to their plane, II. *Proc. Roy. Soc.* **202A,** 81–96.

Ottino, J. M., Ranz, W. E. and Macosko, C. W. (1979) A lamellar model for analysis of liquid–liquid mixing. *Chemical Engineering Science* **34,** 877–890.

Ottino, J. M. (1989) *The Kinematics of Mixing: Stretching, Chaos and Transport*. Cambridge University Press, New York.

Read, K. I. (1984) Experimental investigation of turbulent mixing by Rayleigh–Taylor instability. *Physica* **12D,** 45–58.

Patankar, S. V. and Spalding, D. B. (1972) A calculation procedure for heat, mass and momentum transfer in three-dimensional parabolic flows. *Int. J. Heat and Mass Transfer* **15,** 1787–1806.

Spalding, D. B. (1984) Two-fluid models of turbulence. NASA, Longley Workshop of Theoretical Approaches to Turbulence, Hampton, Virginia.

Taylor, G. I. (1950) The instability of liquid surfaces when accelerated in a direction perpendicular to their plane, I. *Proc. Roy. Soc.* **201A,** 192–196.

Youngs, D. L. (1984) Numerical simulation of turbulent mixing by Rayleigh–Taylor instability. *Physica* **12D,** 32–44.

Youngs, D. L. (1989) Modelling turbulent mixing by Rayleigh–Taylor instability. *Physica* **37D,** 270–287.